Commun. Comput. Phys.
doi: 10.4208/cicp.OA-2016-0088

Vol. **22**, No. 3, pp. 829-851
September 2017

A Third Order Adaptive ADER Scheme for One Dimensional Conservation Laws

Yaguang Gu[1] and Guanghui Hu[1,2,*]

[1] *Department of Mathematics, University of Macau, Macao SAR, China.*
[2] *UM Zhuhai Research Institute, Zhuhai, Guangdong, China.*

Received 15 June 2016; Accepted (in revised version) 16 February 2017

Abstract. We introduce a third order adaptive mesh method to arbitrary high order Godunov approach. Our adaptive mesh method consists of two parts, i.e., mesh-redistribution algorithm and solution algorithm. The mesh-redistribution algorithm is derived based on variational approach, while a new solution algorithm is developed to preserve high order numerical accuracy well. The feature of proposed Adaptive ADER scheme includes that 1). all simulations in this paper are stable for large CFL number, 2). third order convergence of the numerical solutions is successfully observed with adaptive mesh method, and 3). high resolution and non-oscillatory numerical solutions are obtained successfully when there are shocks in the solution. A variety of numerical examples show the feature well.

AMS subject classifications: 35L65, 35L67, 58J45, 35Q31, 65M08

Key words: ADER scheme, adaptive mesh method, finite volume method, WENO reconstruction, hyperbolic equations.

1 Introduction

Hyperbolic conservation laws play an important role in the computational fluid dynamics. A number of numerical methods have been developed to solve the conservation laws such as finite volume method (FVM) [12, 21, 38], discontinuous Galerkin method (DG) [26, 36], Runge-Kutta discontinuous Galerkin method (RKDG) [16, 24, 39, 40], hybridizable discontinuous Galerkin method (HDG) [6, 8], finite element method (FEM) [5, 23], spectral volume method [18, 19]. Recently, high order numerical methods attract more and more attention since their potential on delivering more efficient and accurate solutions [13,32,37]. A variety of limiting strategies have also been developed in the solution reconstruction to deliver high resolution and non-oscillatory numerical solutions, such as

*Corresponding author. *Email addresses:* umacgyg@gmail.com (Y. G. Gu), garyhu@umac.mo (G. H. Hu)

 ©2017 Global-Science Press

https://doi.org/10.4208/cicp.OA-2016-0088 Published online by Cambridge University Press

minmod [9, 20], total variation diminishing method (TVD) and total variation bounded method (TVB) [7, 10], essentially non-oscillatory scheme (ENO) and weighted essentially non-oscillatory scheme (WENO) [2, 4, 27, 29].

Among those high order numerical methods, WENO scheme is one of popular techniques to deliver non-oscillatory reconstructions. However, the optimal CFL number used in the simulation should be less than 0.5, based on numerical experience. At the same time, the WENO reconstruction should be realized three times in one temporal step if third order Runge-Kutta method is applied, for example. In order to speed up the evolution, an arbitrary high order Godunov approach (ADER) was first proposed by E.F. Toro's group [25]. A lot of further researches have been done on linear and non-linear equations, such as advection equation, Burgers equation and Euler system, on one-, two-, and three-dimension cases [31, 32]. To evaluate the numerical flux in the ADER scheme, one solves the generalized Riemann problem (GRP) [33–35]. In this procedure, Taylor expansion of the solution of GRP is performed at the interface, including a leading term and its temporal derivatives. Then all temporal derivatives are expressed in terms of spatial derivatives via Cauchy-Kowalewski procedure, which is the key idea of ADER scheme so that arbitrary high order convergence in temporal discretization can be achieved. Finally one evaluates the leading term by solving a classic Riemann problem and evaluates spatial derivatives by solving a sequence of linearized Riemann problems, respectively, at each cell interface to obtain all terms needed in the Cauchy-Kowalewski procedure and Taylor expansion, where the initial states of these Riemann problems are provided by WENO reconstruction. As was shown in their papers that the desired order convergence of ADER scheme could be achieved when linear and non-linear equations were tested. Besides, the optimal stable CFL number about 1.0 could be chosen, which sped up the evolution.

In [4], a sub-cell WENO reconstruction was proposed for ADER scheme. Numerical experiments therein successfully demonstrated the high order and non-oscillatory features of the numerical solutions. It was noted that in the simulation of Sod problem in that paper, obvious undershoot phenomenon could be observed when ADER scheme was directly used with WENO scheme proposed by Jiang and Shu (WENOJS) [29]. This phenomenon happened when the discontinuous initial condition was resolved exactly by the mesh grids, i.e., when there was a grid point appearing at the discontinuity point. Even worse, this undershoot phenomenon could not be improved by reducing the size of the mesh grids systematically. The explanation they gave in [4] is that the approximation to the leading term has much higher order accuracy than that required by the ADER scheme. We also find that this undershoot phenomenon can be significantly improved when there is an element across the discontinuity point of the initial solution. Finite volume methods propagate cell averages in the time evolution of the system. This means that an artificial smoothing for the initial condition is introduced if we let an element in the mesh cross the discontinuity point, which is negative on the reliability of the simulations. To reduce the gap between the artificially smoothed initial condition and the original one, sufficiently dense mesh grids become necessary.

https://doi.org/10.4208/cicp.OA-2016-0088 Published online by Cambridge University Press

In this paper, an adaptive mesh method is introduced to avoid the high demanding on the computational resource when the uniform mesh is employed. Adaptive mesh method contains two parts: mesh algorithm and solution algorithm. The mesh algorithm is discussed based on the study of variational approach [3, 15, 23, 28, 30]. In those papers, the first and second order solution algorithms were proposed, while higher order solution algorithm should be devised to match the accuracy of ADER scheme. In our paper, we follow their mesh algorithm and at the same time, design a third order solution algorithm. In [11], higher order solution algorithm was proposed, where ENO reconstruction was performed on each old control volume, and solutions were updated on the new control volumes based on those reconstruction polynomials. In our previous work [12, 14], a new robust WENO reconstruction was used on unstructured mesh, where all linear weights were replaced by unity. Once adaptive mesh method is applied, the mesh will become non-uniform. Thus we still use that new robust WENO reconstruction in our solution algorithm. Besides, the same simplification is also used in reconstruction procedure of ADER scheme since the global error is third order.

The rest of this paper is organized as follows. In Section 2, we review the profile of the ADER scheme and its related details: Cauchy-Kowalewski procedure, WENO schemes (WENOJS and WENOZ [2]) and derivative Riemann problems. In Section 3, adaptive mesh method is recalled and we introduce the framework of our third order solution algorithm. Numerical examples are presented in Section 4 to demonstrate the performance and convergence of our method. Finally, the concluding remarks of this paper is given in Section 5.

2 ADER scheme

In this section, we briefly review the profile of the one dimensional ADER scheme and look back over some details in the rest subsections.

The hyperbolic system in conservation laws that we consider in this paper is given by

$$\partial_t u+\partial_x F(u)=0, \tag{2.1}$$

where u is the unknown, and $F(u)$ is the physical flux. Note that u can be either a scalar or a vector.

Now consider a non-uniform mesh grids defined on domain $[a,b]$: $a=x_{1/2}<x_{3/2}<\cdots<x_{N+1/2}=b$. Denote the ith grid cell by

$$I_i=(x_{i-1/2},x_{i+1/2}),\quad i=1,2,\cdots,N.$$

Integrating (2.1) over $[t^n,t^{n+1}]\times[x_{i-1/2},x_{i+1/2}]$ gives the following relationship between two temporal steps:

$$\bar{u}_i^{n+1}=\bar{u}_i^n+\frac{\Delta t}{\Delta x_i}(F_{i-1/2}-F_{i+1/2}), \tag{2.2}$$

https://doi.org/10.4208/cicp.OA-2016-0088 Published online by Cambridge University Press

where

$$\bar{u}_i^n = \frac{1}{\Delta x_i}\int_{x_{i-1/2}}^{x_{i+1/2}} u(t^n,x)dx,$$
$$F_{i\pm1/2} = \frac{1}{\Delta t}\int_{t^n}^{t^{n+1}} F(u(t,x_{i\pm1/2}))dt,$$

with $\Delta x_i = x_{i+1/2} - x_{i-1/2}$. $\bar{u}_i^n$ is the cell average of the solution in cell $[x_{i-1/2}, x_{i+1/2}]$ at time lever t^n, and $F_{i\pm1/2}$ are time averages of the physical fluxes at cell interfaces $x = x_{i\pm1/2}$.

The ADER approach defines numerical fluxes in such a way that the one-step formula (2.2) gives solutions to arbitrary high order convergence in both of space and time. In our paper, we mainly discuss the third order ADER scheme. Algorithm 1 gives the framework of third order ADER scheme. Related details will be introduced in the rest subsections.

Algorithm 1 Framework of ADER3 Scheme.

1: Perform Taylor expansion of u with respect to t and truncate at the second order term:

$$u(\tau,x) \approx u(0^+,x) + \sum_{k=1}^{2} \partial_t^{(k)} u(0^+,x)\frac{\tau^k}{k!}, \tag{2.3}$$

where u is the solution of the GRP (2.14) and τ is local time.

2: Replace all temporal derivatives by spatial derivatives via Cauchy-Kowalewski procedure (2.5). See Section 2.1.

3: Obtain reconstruction polynomial on each control volume and evaluate left and right states at interface by WENO scheme. The WENOJS scheme and WENOZ scheme will be shown in Section 2.2.

4: Solve (2.16) and (2.17) at each interface $x = x_{i+1/2}$ to obtain the leading term of (2.3) and spatial derivatives needed in Cauchy-Kowalewski procedure, respectively. See Section 2.3.

5: Compute $u(\tau_l, x_{i+1/2})$ by using (2.3), where τ_l is Gauss node at the interface.

6: Get numerical fluxes by Gauss quadrature formula:

$$F_{i+1/2} \approx \sum_{l=1}^{K_l} F(u(\tau_l, x_{i+1/2}))\omega_l, \tag{2.4}$$

where K_l is the number of nodes, τ_l and ω_l are properly scaled node and weight of the rule, respectively.

7: Form the scheme (2.2).

https://doi.org/10.4208/cicp.OA-2016-0088 Published online by Cambridge University Press

2.1 Cauchy-Kowalewski procedure

Let N_e denote the number of equations to be solved in (2.1). For the ADER3 scheme, all temporal derivatives are replaced by spatial derivatives according to (2.1) through the Cauchy-Kowalewski procedure:

$$\begin{aligned} u_t &= -F'(u)u_x, \\ u_{tx} &= -(F'(u)u_x)_x = -[F''(u)u_x]u_x - F'(u)u_{xx}, \\ u_{tt} &= -(F'(u)u_x)_t = -[F''(u)u_t]u_x - F'(u)u_{xt} \\ &= \{F''(u)[F'(u)u_x]\}u_x + F'(u)\{[F''(u)u_x]u_x + F'(u)u_{xx}\}, \end{aligned} \tag{2.5}$$

where

$$F'(u)[i][j] = \frac{\partial F_i}{\partial u_j}, \quad i,j = 1,2,\cdots,N_e,$$

$$F''(u)[i][j][k] = \frac{\partial^2 F_i}{\partial u_j \partial u_k}, \quad i,j,k = 1,2,\cdots,N_e.$$

The product of $F''(u)$ and any vector $\overrightarrow{\alpha}$ in (2.5) follows

$$(F''(u)\overrightarrow{\alpha})[i][j] = \sum_{k=1}^{N_e} F''(u)[i][j][k]\overrightarrow{\alpha}[k]. \tag{2.6}$$

2.2 Weighted Essentially Non-Oscillatory schemes

In this section we review the framework of the fifth order finite volume WENOJS scheme and WENOZ scheme [2, 17, 29].

Based on the mesh, a desired order reconstruction polynomial is obtained on each control volume I_i, $i = 1,2,\cdots,N$, by means of WENO scheme, which is prescribed as follows.

Let $(2r-1)$ denote the order of the WENO scheme (In this paper, $r = 3$). $(2r-1)$ volumes, $I_{i-r+1}, I_{i-r+2}, \cdots, I_{i+r-1}$, are used as the global stencil, denoted by S^{2r-1}, which is subdivided into r substencils $S_0, S_1, \cdots, S_{r-1}$, with each of substencils containing r volumes, i.e., $S_k = \{I_{i+k-r+1}, \cdots, I_{i+k}\}$, $k = 0,1,\cdots,r-1$. For example, the stencils used in the fifth order WENO scheme are shown in Fig. 1.

As is shown in [29], on each substencil, a $(r-1)$th order polynomial can be reconstructed

$$p_k^r(x) = \sum_{l=0}^{r-1} R_{k,l}^r(x_{i+k-r+1/2}, \cdots, x_{i+k+1/2}, \bar{u}_{i+k-r+1}, \cdots, \bar{u}_{i+k})x^l, \tag{2.7}$$

such that

$$\frac{1}{\Delta x_j}\int_{I_j} p_k^r(x)dx = \bar{u}_j,$$

https://doi.org/10.4208/cicp.OA-2016-0088 Published online by Cambridge University Press

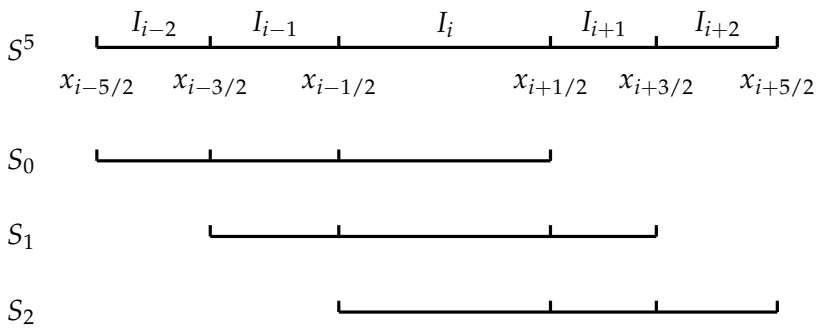


Figure 1: The grid points, stencil S^5 and its substencils S_0, S_1, S_2, used for fifth order WENO reconstruction.

for $k=0,1,\cdots,r-1$, $j=i+k-r+1,\cdots,i+k$. Furthermore, when solution is sufficiently smooth, r substencils can be combined to construct a $(2r-2)$th order approximation polynomial, which is reasonable since $(2r-1)$ volumes are used therein. In order to realize it, a linear combination of all the reconstruction polynomials on S^{2r-1} are developed

$$p^{2r-1}(x)=\sum_{k=0}^{r-1}d_k(x)p_k^r(x), \tag{2.8}$$

where d_k, $k=0,1,\cdots,r-1$, are called the optimal weights, depending on the position of the point where function value is evaluated. We refer to [29] for d_k, $k=0,1,\cdots,r-1$, when the mesh is uniform. When discontinuity appears, some constraints should be added to d_k, $k=0,1,\cdots,r-1$, to guarantee that the substencil which contains discontinuity should contribute little to the reconstruction. Thus the reconstruction polynomial is revised into the following form:

$$p^{2r-1}(x)=\sum_{k=0}^{r-1}\omega_k(x)p_k^r(x), \tag{2.9}$$

where ω_k, $k=0,1,\cdots,r-1$, are non-linear weights.

For the WENOJS scheme, the non-linear weights are given by the following way:

$$\omega_k=\frac{\alpha_k(x)}{\sum_{l=0}^{r-1}\alpha_l(x)},\quad \alpha_k=\frac{d_k(x)}{(\beta_k+\epsilon)^p},\quad k=0,1,\cdots,r-1, \tag{2.10}$$

where p is a positive number and $\epsilon>0$ is used to prevent the denominator from 0. In this paper we take $p=2$, $\epsilon=10^{-6}$. β_k is expressed by the following integral, indicating the smoothness of reconstruction polynomial on the kth substencil

$$\beta_k=\sum_{l=1}^{r-1}\int_{i-1/2}^{i+1/2}(\Delta x)^{2l-1}\left(\frac{\partial^l p_k^r(x)}{\partial x^l}\right)^2 dx. \tag{2.11}$$

https://doi.org/10.4208/cicp.OA-2016-0088 Published online by Cambridge University Press

Specially when the mesh is uniform, a more accurate WENOZ scheme can be derived, where the smoothness indicator is given by:

$$\alpha_k = d_k\left(1+\left(\frac{\tau_{2r-1}}{\beta_k+\epsilon}\right)^2\right), \quad k=0,1,\cdots,r-1, \tag{2.12}$$

where τ is discussed in [2]. In the case of $r=3$, τ satisfies

$$\tau_5 = |\beta_2-\beta_0|. \tag{2.13}$$

2.3 Derivative Riemann problem

In this section, we review the Riemann problems considered in ADER scheme [33,34].

After the reconstruction step the conservative variables on each cell are represented by vector polynomials $p_i(x)$, $i=1,2,\cdots,N$. Then at each interface, the following GRP is proposed:

$$\begin{aligned} &\partial_t u+\partial_x F(u)=0,\\ &u(x,0)=\begin{cases} u_L(x)=p_i(x), & x<x_{i+1/2},\\ u_R(x)=p_{i+1}(x), & x>x_{i+1/2}. \end{cases} \end{aligned} \tag{2.14}$$

In order to obtain an approximate solution for the interfacial state $u(\tau,x_{i+1})$, where τ is local time $\tau=t-t^n$, Taylor expansion of the interfacial state is performed:

$$u(\tau,x_{i+1/2}) \approx u(0^+,x_{i+1/2})+\sum_{k=1}^{2}\partial_t^{(k)}u(0^+,x_{i+1/2})\frac{\tau^k}{k!}, \tag{2.15}$$

where

$$\partial_t^{(k)}u(0^+,x_{i+1/2})=\partial_t^{(k)}u(t,x)|_{(0^+,x_{i+1/2})}, \quad 0^+=\lim_{t\to(t^n)^+}t.$$

The approximate solution depends on a leading term $u(0^+,x_{i+1/2})$ and higher order terms with coefficients determined by temporal derivatives $\partial_t^{(k)}u(0^+,x_{i+1/2})$. By (2.5), we need to evaluate the leading term and higher order spatial derivatives at interface. In the following subsections, the methods to compute each of these terms are stated.

2.3.1 The leading term

The leading term $u(0^+,x_{i+1/2})$ accounts for the first-instance interaction at the interface. The boundary extrapolated values u_L and u_R are set as the Godunov states of GRP:

$$\begin{aligned} &\partial_t u+\partial_x F(u)=0,\\ &u(x,0)=\begin{cases} u_L=\lim\limits_{x\to x_{i+1/2}^-}p_i(x), & x<x_{i+1/2},\\ u_R=\lim\limits_{x\to x_{i+1/2}^+}p_{i+1}(x), & x>x_{i+1/2}. \end{cases} \end{aligned} \tag{2.16}$$

https://doi.org/10.4208/cicp.OA-2016-0088 Published online by Cambridge University Press

The leading term is obtained by solving the above PDE. In practise, u_L and u_R are directly evaluated by WENO scheme. We refer to [22,33] for Riemann solvers. For the linear problem such as advection equation and quasi-linear problem such as Burgers equation, direct solver can be used. For the Euler system, we use an approximate HLLC Riemann solver since the eigenstructure of Euler system always has an intermediate contact wave, which is incorporated by HLLC Riemann solver.

2.3.2 Higher Order Terms

Differentiate the governing equation (2.1) with respect to x, we obtain

$$\partial_t(\partial_x^{(k)}u)+A(u)\partial_x(\partial_x^{(k)}u)=H(u,\partial_x^{(1)}u,\partial_x^{(2)}u,\cdots,\partial_x^{(k-1)}u), \tag{2.17}$$

where H is a function formed after moving the terms with lower order derivatives to the right hand side.

However, it is not convenient to solve these PDEs for 1). they are non-linear and 2). the source terms are involved. In order to make it easier to get these higher order terms, two simplifications are made without destroying the high order of the numerical scheme [34], i.e. 1). The source term $H(u,\partial_x^{(1)}u,\partial_x^{(2)}u,\cdots,\partial_x^{(k-1)}u)$ is neglected since the spatial derivatives are only in need of the first-instance interaction of its neighbour states. 2). The coefficient matrix $A(u)$ is linearized by $u(0^+,x_{i+1/2})$, which is obtained by solving (2.16). Then higher order terms are obtained by solving the following LRP:

$$\begin{aligned}&\partial_t(\partial_x^{(k)}u)+A\partial_x(\partial_x^{(k)}u)=0,\\ &\partial_x^{(k)}u(x,0)=\begin{cases}\partial_x^{(k)}u_L=\lim\limits_{x\to x_{i+1/2}^-}\partial_x^{(k)}p_i(x), & x<x_{i\pm1/2},\\ \partial_x^{(k)}u_R=\lim\limits_{x\to x_{i+1/2}^+}\partial_x^{(k)}p_{i+1}(x), & x>x_{i\pm1/2},\end{cases}\end{aligned} \tag{2.18}$$

where $A=F'(u(0^+,x_{i+1/2}))$. Note that the coefficient matrix A is same for all spatial derivatives $\partial_x^{(k)}u$ at each interface, and needs to be evaluated only once. In practise, $\partial_x^{(k)}u_L$ and $\partial_x^{(k)}u_R$ are evaluated directly by differentiating the same WENO reconstruction polynomial. The Riemann solvers of (2.18) are as follows:

- For scalar problems, we solve the problems directly.
- Note that for the Euler equations, (2.18) is already a linear system. Several strategies are available to solve this system. Particularly we choose the one as follows. We first transform conservative variables by characteristic projection, then solve the problem directly in characteristic space, and finally project solutions back [33].

https://doi.org/10.4208/cicp.OA-2016-0088 Published online by Cambridge University Press

3 Third order adaptive mesh method

In the simulation of hyperbolic equations which contain discontinuities, resolving these discontinuities accurately and effectively is crucial. Adaptive mesh method is an efficient tool to capture the structures of hyperbolic problems. Adaptive mesh method contains two parts: mesh-redistribution algorithm and solution algorithm. In this section, we first revisit mesh-redistribution algorithm in Section 3.1 and then introduce our solution algorithm in Section 3.2.

3.1 Mesh-redistribution algorithm

In this section, we revisit mesh-redistribution algorithm delivered in [30].

The mesh-redistribution algorithm is based on the variational approach. Let x and ξ denote the physical and computational coordinates, respectively. A bijective coordinate transformation from the computational domain $\Omega_c=[0,1]$ to the physical domain $\Omega_p=[a,b]$ is given by

$$\begin{aligned} &x=x(\xi), \quad \xi\in\Omega_c, \\ &x(0)=a, \quad x(1)=b. \end{aligned} \tag{3.1}$$

In one dimensional case, the mesh map is provided by the minimizer of a functional, which is defined as the energy of the mesh and has the following form

$$E(\xi)=\frac{1}{2}\int_{\Omega_p}\frac{1}{\omega}(\xi_x)^2dx, \tag{3.2}$$

where ω is called the monitor function, related to the underlying solutions to be adapted. The Euler-Lagrange equation, of which the solution minimizes (3.2), is given by

$$(\omega^{-1}\xi_x)_x=0.$$

The above equation yields the conventional equidistribution principle: $\omega x_\xi=$ constant, or equivalently

$$(\omega x_\xi)_\xi=0. \tag{3.3}$$

An artificial temporal term τ is introduced so that (3.3) can be solved efficiently. Eventually we solve

$$x_\tau=(\omega x_\xi)_\xi, \quad 0<\xi<1, \tag{3.4}$$

with the boundary condition $x(0,\tau)=a$ and $x(1,\tau)=b$. To solve (3.4), the following full discretization on the uniform mesh in computational domain could be adopted:

$$x_{j+1/2}^{[\nu+1]}=x_{j+1/2}^{[\nu]}+\frac{\Delta\tau}{\Delta\xi^2}[\omega(\bar{u}_{j+1}^{[\nu]})(x_{j+3/2}^{[\nu]}-x_{j+1/2}^{[\nu]})-\omega(\bar{u}_j^{[\nu]})(x_{j+1/2}^{[\nu]}-x_{j-1/2}^{[\nu]})], \tag{3.5}$$

https://doi.org/10.4208/cicp.OA-2016-0088 Published online by Cambridge University Press

or in iterative point of view, the following Gauss-Seidel-type iteration also solves (3.4):

$$\omega(\bar{u}_{j+1}^{[\nu]})(x_{j+3/2}^{[\nu]}-x_{j+1/2}^{[\nu+1]})-\omega(\bar{u}_{j}^{[\nu]})(x_{j+1/2}^{[\nu+1]}-x_{j-1/2}^{[\nu+1]})=0, \tag{3.6}$$

where $\Delta\xi=1/(N+1)$ is the step size in Ω_c; $x^{[\nu]}$, $\bar{u}^{[\nu]}$ and $x^{[\nu+1]}$, $\bar{u}^{[\nu+1]}$ represent the distributions of the mesh and cell averages before and after one-step mesh motion, respectively. Denote $\alpha_{j+1}=\frac{\Delta\tau}{\Delta\xi^2}\omega(\bar{u}_{j+1}^{[\nu]})$. The above algorithms are stable when $\max_j\{\alpha_{j+1}\}\leq\frac{1}{2}$.

Note that the accuracy of adaptive mesh method is mainly determined by solution algorithm, i.e. the effect on accuracy by the gap between good approximate and exact solutions of (3.4) could be ignored. Thus we do not need to solve (3.4) until its steady solution. In most test problems, the grid points updating procedure takes five full Gauss-Seidel iterations at each time step, shown in [30].

Furthermore, the authors in [30] also proved that algorithms (3.5) and (3.6) satisfy the following important properties:

$$\begin{aligned}
&x_{1/2}^{[\nu+1]}=x_{1/2}^{[\nu]},\quad x_{N+1/2}^{[\nu+1]}=x_{N+1/2}^{[\nu]},\\
&x_{i-1/2}^{[\nu+1]}<x_{i+1/2}^{[\nu+1]},\quad i=1,\cdots,N\\
&x_{i-1/2}^{[\nu]}<x_{i+1/2}^{[\nu+1]}<x_{i+3/2}^{[\nu]},\quad i=1,\cdots,N-1.
\end{aligned} \tag{3.7}$$

Note the second line of (3.7) indicates that the mesh generated by above two mesh-redistribution algorithm will not overlap. Furthermore, the third line shows that each new inner mesh grid locates only in the neighbour volumes and hence can be applied to design solution algorithm (3.9).

In this paper, we follow their Gauss-Seidel-type mesh-redistribution algorithm.

3.2 Solution algorithm

In solution updating procedure, we hope to reconstruct piecewise desired order polynomials on each new cell and then update the cell averages. To realize it, we need to obtain reconstruction polynomial on each old cell, see Fig. 2. Different from WENO reconstruction, we can not expect reconstruction polynomial to achieve higher order convergence because the linear weights can not be determined on the entire control volume (They depend on the position of a point, where the function value is evaluated). In [11], a desired order polynomial is reconstructed on each cell by ENO scheme, where the smoothest stencil is chosen. In our previous work [12], a new robust WENO reconstruction procedure is devised, where all linear weights d_k are dropped, i.e., the indicator ω_k is evaluated by

$$\omega_k=\frac{\alpha_k(x)}{\sum_{l=0}^{r-1}\alpha_l(x)},\quad \alpha_k=\frac{1}{(\beta_k+\epsilon)^p},\quad k=0,1,\cdots,r-1. \tag{3.8}$$

In this paper, we apply the same way of reconstruction used in our previous work in the solution algorithm. Meanwhile, the same simplification, i.e., the new smooth indicator,

https://doi.org/10.4208/cicp.OA-2016-0088 Published online by Cambridge University Press

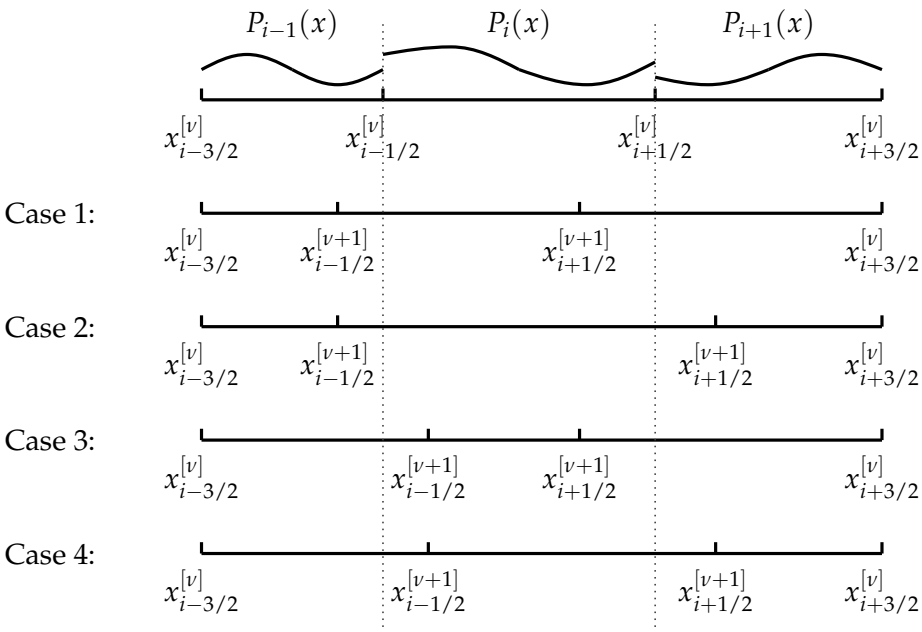


Figure 2: Above: The old grid points and the reconstruction polynomials. Below: Four possible distributions of the new grid points.

is also applied to Step 3 in Algorithm 1 when adaptive mesh method is applied since the global error is third order.

Based on (3.7), solutions are updated by computing the cell averages of reconstruction polynomials on each control volume once the positions of new grid points are verified. For the ith volume, $i=1,2,\cdots,N$, for example, there are four possible distributions of $x^{[\nu+1]}_{i-1/2}$ and $x^{[\nu+1]}_{i+1/2}$, see Fig. 2. After the distributions of $x^{[\nu+1]}_{i-1/2}$ and $x^{[\nu+1]}_{i+1/2}$ are verified, we update new cell average in the following way:

$$
\begin{aligned}
&Case1: \quad \bar{u}_i^{[\nu+1]} = \frac{1}{\Delta x_i^{[\nu+1]}} \left(\int_{x^{[\nu+1]}_{i-1/2}}^{x^{[\nu]}_{i-1/2}} P_{i-1}(x)dx + \int_{x^{[\nu]}_{i-1/2}}^{x^{[\nu+1]}_{i+1/2}} P_i(x)dx \right),\\
&Case2: \quad \bar{u}_i^{[\nu+1]} = \frac{1}{\Delta x_i^{[\nu+1]}} \left(\int_{x^{[\nu+1]}_{i-1/2}}^{x^{[\nu]}_{i-1/2}} P_{i-1}(x)dx + \int_{x^{[\nu]}_{i-1/2}}^{x^{[\nu]}_{i+1/2}} P_i(x)dx + \int_{x^{[\nu]}_{i+1/2}}^{x^{[\nu+1]}_{i+1/2}} P_{i+1}(x)dx \right),\\
&Case3: \quad \bar{u}_i^{[\nu+1]} = \frac{1}{\Delta x_i^{[\nu+1]}} \int_{x^{[\nu+1]}_{i-1/2}}^{x^{[\nu+1]}_{i+1/2}} P_i(x)dx,\\
&Case4: \quad \bar{u}_i^{[\nu+1]} = \frac{1}{\Delta x_i^{[\nu+1]}} \left(\int_{x^{[\nu+1]}_{i-1/2}}^{x^{[\nu]}_{i+1/2}} P_i(x)dx + \int_{x^{[\nu]}_{i+1/2}}^{x^{[\nu+1]}_{i+1/2}} P_{i+1}(x)dx \right).
\end{aligned}
\tag{3.9}
$$

In each time step we perform our adaptive mesh method illustrated by Algorithm 2 and then evolve the problem to the next time step by ADER approach. More atten-

https://doi.org/10.4208/cicp.OA-2016-0088 Published online by Cambridge University Press

tion should be paid at the beginning time step that we update solutions based on the initial condition rather than (3.9). By this means we retain the initial condition when it is smooth, or only change a little the initial condition by averaging it on the element across the discontinuity. Thus this kind of artificial smoothing gives more possibilities that ADER scheme delivers non-oscillatory results.

Algorithm 2 Framework of Adaptive Mesh Method.

INPUT:

Old grid points $\{x_{i+1/2}\}$ of the domain and the cell averages $\{\bar{u}_i\}$ at $t=t^n$.

OUTPUT:

New grid points $\{\tilde{x}_{i+1/2}\}$ and cell averages $\{\tilde{\bar{u}}_i\}$ at $t=t^n$.

1: Define $x_{i+1/2}^{[0]}=x_{i+1/2}$, $\bar{u}_i^{[0]}=\bar{u}_i$.
2: Let $\nu=0$.
3: **while** $\nu<5$ **do**
4: Perform new robust WENO procedure to obtain reconstruction polynomials on the mesh.
5: Use (3.6) to move the grid point from $\{x_{i+1/2}^{[\nu]}\}$ to $\{x_{i+1/2}^{[\nu+1]}\}$. Update the solution based on the old and new grid points by (3.9).
6: $\nu=\nu+1$.
7: **end while**
8: $\tilde{x}_{i+1/2}=x_{i+1/2}^{[\nu]}$, $\tilde{\bar{u}}_i=\bar{u}_i^{[\nu]}$.

4 Numerical experiments

In this section, the accuracy and performances of ADER-WENOJS scheme and ADER-WENOZ scheme will be tested. We will also show the accuracy and performances when adaptive mesh method is applied to ADER scheme (Adaptive ADER).

4.1 Advection equation

The advection equation considered in this paper is given by

$$\begin{aligned} &u_t+F(u)_x=0,\\ &u(0,x)=u_0(x), \end{aligned} \tag{4.1}$$

where $F(u)=u$, $u_0(x)=\sin(\pi x)$. The advection equation is solved on $[-1,1]$ with periodic boundary condition, output time $t=1.0$, CFL number is set to be 0.95. The numerical results are shown in Table 1. We observe that both of ADER-WENOJS scheme and ADER-WENOZ scheme achieve the designed order of convergence and perform well.

https://doi.org/10.4208/cicp.OA-2016-0088 Published online by Cambridge University Press

Table 1: Advection equation. Initial condition: $u_0(x)=\sin(\pi x)$. Output Time $t=1.0$, CFL$=0.95$, N is number of cells.

	ADER-WENOJS				ADER-WENOZ			
N	l_2 error	l_2 order	l_∞ error	l_∞ order	l_2 error	l_2 order	l_∞ error	l_∞ order
20	8.73E-5		1.63E-4		9.22E-5		1.30E-4	
40	1.12E-5	2.96	1.89E-5	3.11	1.24E-5	2.89	1.75E-5	2.89
80	1.54E-6	2.86	2.27E-6	3.06	1.58E-6	2.97	2.24E-6	2.97
160	1.97E-7	2.97	2.82E-7	3.01	1.99E-7	2.99	2.81E-7	2.99
320	2.49E-8	3.17	3.53E-8	3.00	2.50E-8	2.99	3.53E-8	2.99

4.2 Burgers equation

The inviscid Burgers equation considered in this paper is given by

$$\begin{aligned} &u_t+F(u)_x=0,\\ &u(0,x)=u_0(x), \end{aligned} \tag{4.2}$$

where $F(u)=\frac{1}{2}u^2$, $u_0(x)=0.25+0.5\sin(\pi x)$. The Burgers equation is solved on $[-1,1]$ with periodic boundary condition, output time $t=0.2$. In the simulation, CFL number is set to be 0.95. The numerical results are shown in Table 2. We observe that both of ADER-WENOJS scheme and ADER-WENOZ scheme achieve the designed order of convergence and perform well.

Table 2: Burgers equation. Initial condition: $u_0(x)=0.25+0.5\sin(\pi x)$. Output Time $t=0.2$, CFL$=0.95$, N is number of cells.

	ADER-WENOJS				ADER-WENOZ			
N	l_2 error	l_2 order	l_∞ error	l_∞ order	l_2 error	l_2 order	l_∞ error	l_∞ order
40	7.48E-5		2.05E-4		7.46E-5		1.97E-4	
80	9.72E-6	2.94	2.84E-5	2.85	9.74E-6	2.94	2.86E-5	2.78
160	1.26E-6	2.95	3.81E-6	2.90	1.26E-6	2.95	3.81E-6	2.91
320	1.65E-7	2.93	5.05E-7	2.92	1.65E-7	2.93	5.06E-7	2.91

4.3 Euler equations

The Euler equations considered in this paper is given by:

$$U_t+F(U)_x=0, \tag{4.3}$$

where

$$U=\begin{pmatrix}\rho\\ \rho u\\ E\end{pmatrix},\quad F(U)=\begin{pmatrix}\rho u\\ \rho u^2+P\\ (E+P)u\end{pmatrix}, \tag{4.4}$$

https://doi.org/10.4208/cicp.OA-2016-0088 Published online by Cambridge University Press

with the equation of state

$$E=\frac{P}{\gamma-1}+\frac{1}{2}\rho u^2. \tag{4.5}$$

Here ρ is the fluid density, u is the fluid velocity, P is the pressure, E is the total energy, and γ is the ratio of specific heats. In the following experiments, γ is set to be 1.4.

Shock turbulence interaction problem , Lax problem and Sod problem are tested in this paper. We first test all problems by ADER scheme. Then for those problems that the ADER scheme can not handle, we will apply Adaptive ADER scheme to solve the problems. The initial conditions and boundary conditions of Shock turbulence interaction problem , Lax problem and Sod problem are as follows:

- For the shock turbulence interaction problem, the left and right initial states of the density ρ, velocity u and pressure p are

$$(\rho,u,p)=\begin{cases}(3.857143, & 2.629369, & 3.333333), & -1\le x<-0.8,\\ (1+0.2\sin(5\pi x), & 0.000000, & 1.000000), & -0.8\le x\le 1,\end{cases} \tag{4.6}$$

  and the output time is $t=0.47$.

- For the Lax problem, the left and right initial constant states of the density ρ, velocity u and pressure p are

$$(\rho,u,p)=\begin{cases}(0.445, & 0.698, & 3.528), & -5\le x<0,\\ (0.500, & 0.000, & 0.571), & 0\le x\le 5,\end{cases} \tag{4.7}$$

  and the output time is $t=1.3$.

- For the Sod problem, the left and right initial constant states of the density ρ, velocity u and pressure p are

$$(\rho,u,p)=\begin{cases}(1.000, & 0.000, & 1.000), & -5\le x<0,\\ (0.125, & 0.000, & 0.100), & 0\le x\le 5,\end{cases} \tag{4.8}$$

  and the output time is $t=2.0$.

Since the computational domains of all the above problems are sufficiently large to contain all the flow structures, free-stream boundary conditions are set at both ends of the computational domain. Note that in this paper, the WENO reconstruction is operated on conservative variables to guarantee conservative properties. Moreover, CFL number set in all of the following simulations is also 0.95.

First we test the shock turbulence interaction problem by ADER-WENOJS scheme and ADER-WENOZ scheme. Fig. 3 shows the results. We can observe the convergence of the ADER-WENOJS scheme and ADER-WENOZ scheme. Meanwhile, it indicates that the both of ADER-WENOJS scheme and ADER-WENOZ scheme perform well when $N=2000$. This is the case that both of ADER schemes can well handle.

https://doi.org/10.4208/cicp.OA-2016-0088 Published online by Cambridge University Press

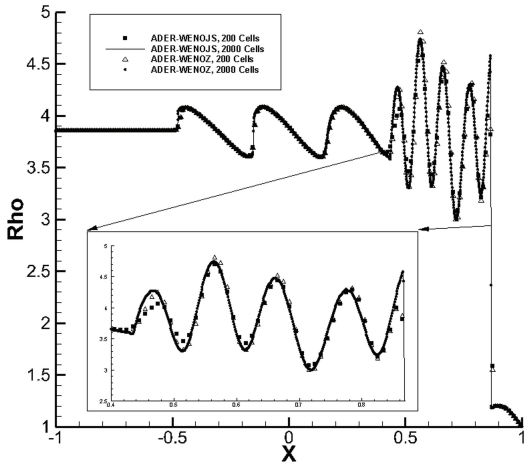


Figure 3: Shock turbulence interaction problem, solved by the ADER-WENOJS scheme and the ADER-WENOZ scheme. Output time $t=0.47$.

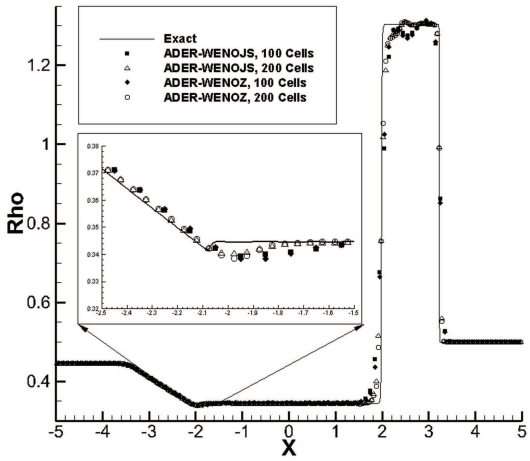


Figure 4: Lax problem, solved by the ADER-WENOJS scheme and the ADER-WENOZ scheme. Output time $t=1.3$. "Exact" Solution: ADER-WENOJS, 2000 Cells.

Later on, the Lax problem is tested by ADER-WENOJS scheme and ADER-WENOZ scheme. We can see from the Fig. 4 that both of the ADER-WENOJS scheme and ADER-WENOZ give convergent solutions. However, non-physical undershoots occur at the tail of rarefaction wave. Besides, oscillations can also be observed between contact discontinuity and shock. Similar results are obtained when we check the Sod problem. As is shown in Fig. 5 that non-physical undershoots appear at the tail of the rarefaction wave, which coincides with the phenomenon observed in [4]. ADER-WENOZ scheme gives more accurate solutions around contact discontinuities and shocks but fails to reduce the

https://doi.org/10.4208/cicp.OA-2016-0088 Published online by Cambridge University Press

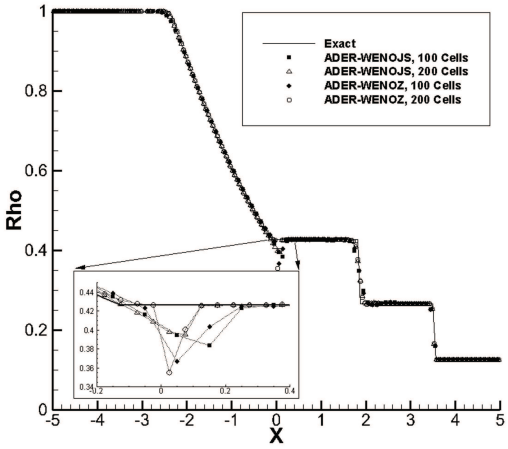


Figure 5: Sod problem, solved by the ADER-WENOJS scheme and the ADER-WENOZ scheme. Output time $t=2.0$. We refer to [1] for the "Exact" Solution.

undershoot. The reasons are two folds: On the one hand, the Godunov approach usually gives such kind of undershoot at the tail of the rarefaction wave. On the other hand, approximation to the leading term in the ADER scheme has much higher order accuracy than that required by the ADER scheme [4]. In fact, the solutions (density, momentum and energy) propagate along the characteristics of hyperbolic equations, and those errors brought in from the beginning, whereafter, will propagate along characteristics and become uncontrolled.

In order to improve the simulation, we test the sod problem with odd number of volumes. Further more, we generalize the mesh and solve the problem on a random mesh. Note that for the random mesh, new robust WENO reconstruction will be used since the problem is solved on non-uniform mesh, and refinement is operated based on the initial random mesh. Fig. 6 and Fig. 7 show the results of our tests. We can see from two figures that when we simulate the problem with odd number of volumes or on a random mesh, solutions become better, with the undershoots well reduced. The reason we find out is that when there is a volume across the discontinuity at the beginning, the initial setup on that volume will be an average of its neighbour states, which can be regarded as a good smooth approximation to the original initial setup. Otherwise the discontinuity will locate at interface, where it is not easy for ADER scheme to handle.

To show the convergence when this kind of initial setup is applied, we just simply solve the following advection equation by the first order Godunov scheme on uniform mesh with odd number of volumes:

$$\begin{aligned} &u_t+u_x=0,\\ &u(0,x)=\begin{cases} 1.0, & -1\le x<0,\\ -1.0, & 0\le x\le 1. \end{cases} \end{aligned} \tag{4.9}$$

Periodic boundary condition is applied, and final time $t=1.0$. Fig. 8 shows the results of

https://doi.org/10.4208/cicp.OA-2016-0088 Published online by Cambridge University Press

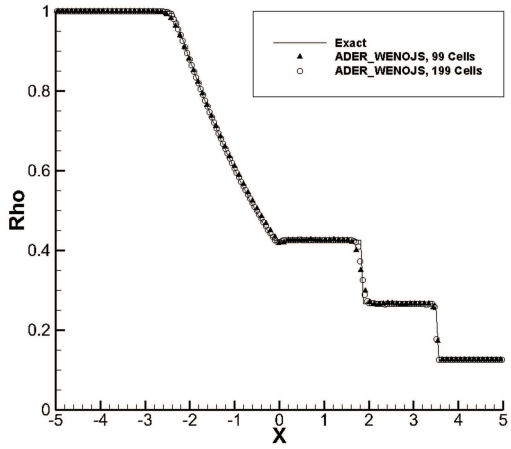


Figure 6: Sod problem, solved by the ADER-WENOJS scheme. Output time $t=2.0$.

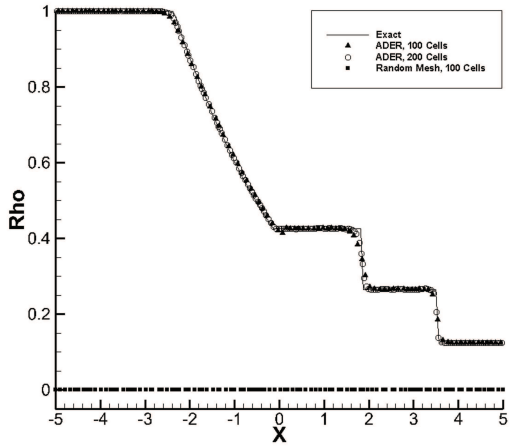


Figure 7: Sod problem, solved by the ADER scheme. Output time $t=2.0$.

the problem. As we refine the mesh, the result becomes more accurate to exact solution, which indicates the convergence of such method. However, denser mesh should be used if we want to get a sharp solution.

Now we sum up the above problems. On the one hand, we aim at reducing the undershoot at the tail of rarefaction wave. A good way to realize it is to have one volume cross the discontinuity from the beginning, which can be regarded as a smooth approximation to initial condition. On the other hand, however, if we use smooth approximation to the initial setup, the mesh size should be sufficiently small to capture each discontinuous structure. Adaptive mesh method is an efficient tool to handle such problems. On the one hand, adaptive mesh method could adaptively redistribute mesh with time so that the mesh will become locally denser near large gradients and discontinuities at each

https://doi.org/10.4208/cicp.OA-2016-0088 Published online by Cambridge University Press

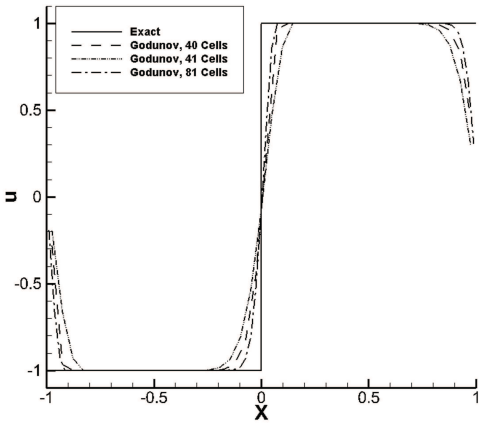


Figure 8: Advection equation, solved by first order Godunov scheme. Output time $t=1.0$.

time step. On the other hand, less number of volumes will handle the problem, which saves the memory.

Before we give solutions of the Lax problem and Sod problem, we first check the convergence of our Adaptive ADER scheme. We still simulate the same problem discussed in Section 4.2. The monitor function used in the simulation is $\omega=\sqrt{1+0.2|u_\xi|^2}$, given in [30], Output Time $t=0.2$, $t=0.3$ and $t=0.4$, CFL$=0.95$. Table 3 shows the convergence rate. We observe that our Adaptive ADER scheme guarantees third order convergence. Fig. 9 shows the mesh motions and results when shock forms. We can see that our algorithm can well capture the position of shock and adaptively redistribute more grid points around it. Besides, solution becomes more accurate to exact solution when $N=80$ than that when $N=50$, which indicates the convergence of Adaptive ADER scheme.

Table 3: Adaptive ADER scheme tested on Burgers equation. L^2-error and convergence order at $t=0.2$, $t=0.3$ and $t=0.4$.

Time \ N	20	40	80	160
$t=0.2$	1.07E-3 (-)	1.00E-4 (3.42)	1.09E-5 (3.20)	1.40E-6 (2.96)
$t=0.3$	2.16E-3 (-)	2.35E-4 (3.20)	2.61E-5 (3.17)	3.28E-6 (2.99)
$t=0.4$	4.57E-3 (-)	5.98E-4 (2.93)	6.65E-5 (3.17)	8.59E-6 (2.95)

Finally we apply Adaptive ADER scheme to solve the Lax problem and Sod problem. The monitor function used in the simulation is $\omega=\sqrt{1+\alpha_1|\rho_\xi|^2+\alpha_2|s_\xi|^2+\alpha_3|\rho_{\xi\xi}|^2}$, where s is entropy, and $\alpha_1=\alpha_2=\alpha_3=100$; ρ_ξ, s_ξ are first derivatives of density and entropy, respectively, and $\rho_{\xi\xi}$ is the second derivative of density. We add term $\rho_{\xi\xi}$ to capture the change of gradient so that denser the grid points will be in the neighbour of discontinuity. Fig. 10 and Fig. 11 show the results of Lax problem and also the mesh motions. We

https://doi.org/10.4208/cicp.OA-2016-0088 Published online by Cambridge University Press

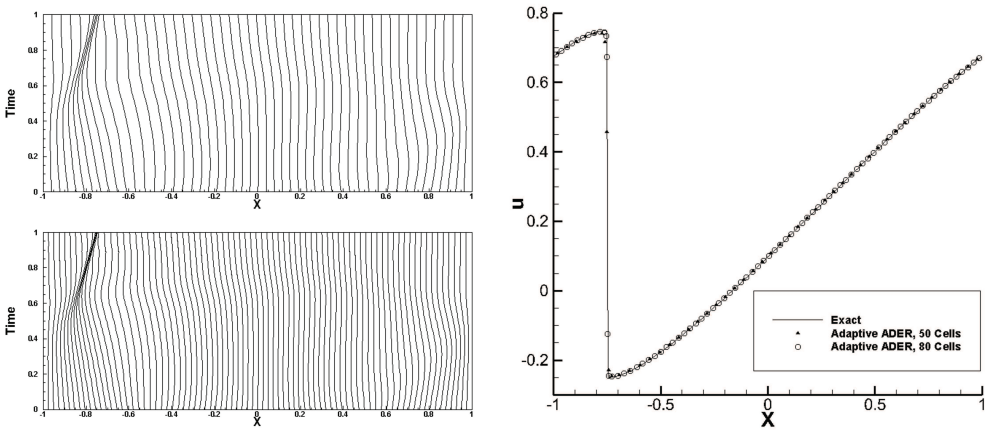


Figure 9: Solutions of Burgers equation by Adaptive ADER scheme, Initial condition: $u_0(x)=0.25+0.5\sin(\pi x)$. Output Time $t=1.0$, CFL$=0.95$, N is number of cells. Left Top: Mesh distribution with $N=50$, Left Bottom: Mesh distribution with $N=80$, and Right: Solutions with $N=50$ and $N=80$. The "exact" solution is computed by ADER-WENOZ scheme with $N=640$.

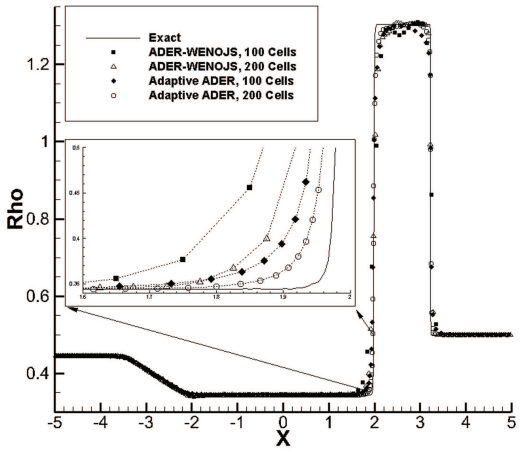


Figure 10: Lax problem, solved by the ADER-WENOJS and the Adaptive ADER scheme. Output time $t=1.3$.

can see from Fig. 10 that the Adaptive ADER scheme gives quite better results at the tail of the rarefaction wave, contact discontinuity and shock, and also reduces the oscillations between contact discontinuity and shock. We also observe in the "zoom in" frame that the result of Adaptive ADER scheme with 100 cells is quite better than that of ADER-WENOJS scheme with 200 cells around discontinuity, which indicates the advantage of adaptive mesh method: resources saving. Convergence of Adaptive ADER scheme is shown in Fig. 11. We can observe in Fig. 11 that the result is better when $N=200$ than that when $N=100$ in the right frame, and structures are better captured on denser mesh shown in the left two frames. Fig. 12 and Fig. 13 shows the results of Sod problem and

https://doi.org/10.4208/cicp.OA-2016-0088 Published online by Cambridge University Press

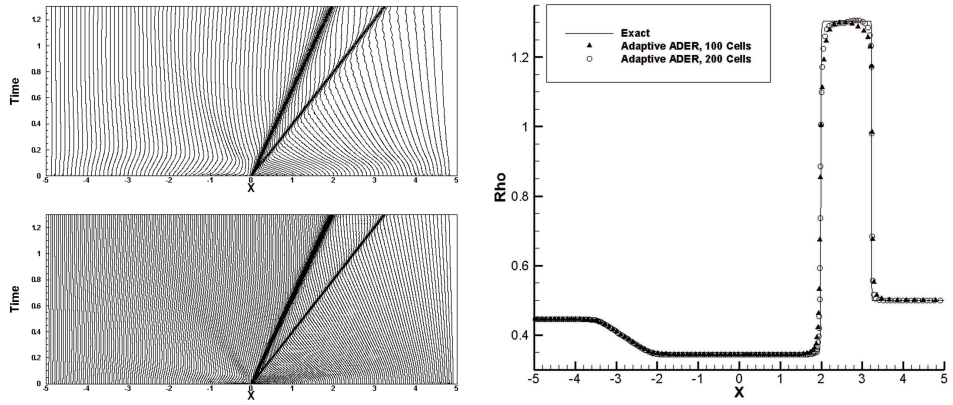


Figure 11: Lax problem, solved by the Adaptive ADER scheme. Output time $t=1.3$. Left: Mesh redistribution with $N=100$ and $N=200$. Right: Solutions of Adaptive ADER scheme.

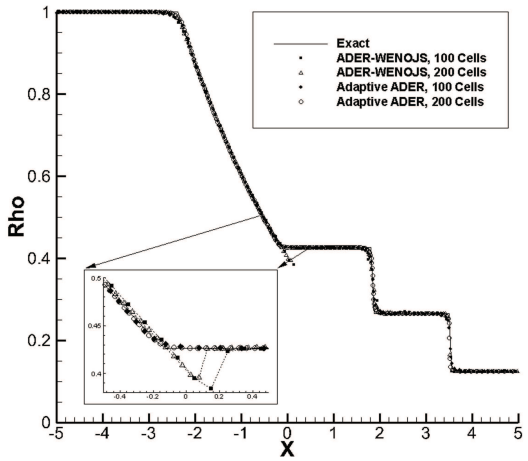


Figure 12: Sod problem, solved by the ADER-WENOJS and the Adaptive ADER scheme. Output time $t=2.0$.

mesh motions. We can see from Fig. 12 that the results of Adaptive ADER scheme are better than that of ADER-WENOJS scheme, especially at the tail of rarefaction wave. Besides, contact discontinuity and shock are also better resolved by Adaptive ADER scheme in the simulation. Convergence of Adaptive ADER scheme can be observed in the right frame of Fig. 13. The left two frames of Fig. 13 show the mesh motions. We can observe that our adaptive mesh method could well detect structures with large gradients and discontinuities, and adaptively redistribute more grid points around them. Further more, the structures are better captured on denser mesh, which indicates the convergence of our method.

In this section, we illustrate our method by testing some of classic models. Our approach on the one hand, greatly reduced the oscillation observed in [4] when ADER

https://doi.org/10.4208/cicp.OA-2016-0088 Published online by Cambridge University Press

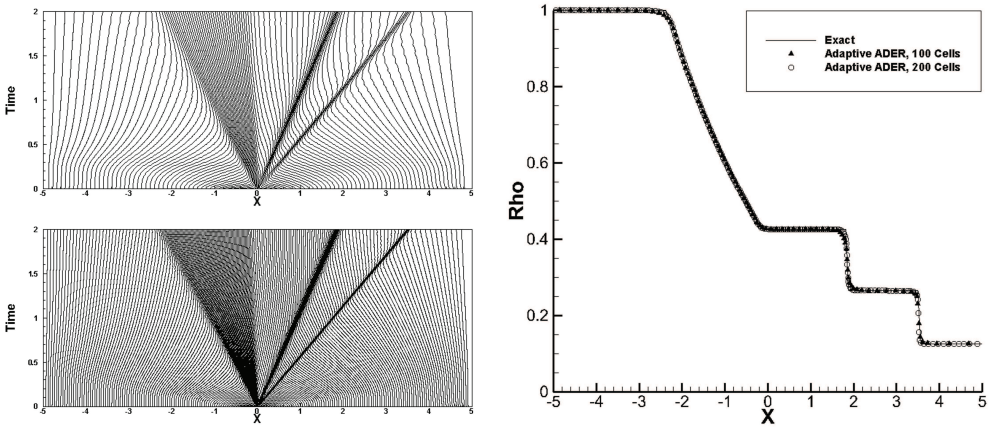


Figure 13: Sod problem, solved by the Adaptive ADER scheme. Output time $t=2.0$. Left: Mesh redistribution with $N=100$ and $N=200$. Right: Solutions of Adaptive ADER scheme.

scheme is directly applied. On the other hand, the CFL number is chosen to be 0.95 in these tests, which retain the strength of ADER scheme that larger (about 1) CFL number can be adopted, compared to some of other classic approaches such as Runge-Kutta WENO scheme, where the ideal CFL number should be less than 0.5 [2, 17].

5 Concluding remarks

In this paper we have tested third order finite volume ADER-WENOJS scheme and ADER-WENOZ scheme, and further devised a third order Adaptive ADER scheme for conservation laws. For smooth solutions, both of ADER-WENOJS scheme and ADER-WENOZ scheme perform well and achieve the desired order of accuracy. However, it is observed that non-physical oscillation will appear around the discontinuity when ADER-WENO schemes are applied. We devise a third order adaptive mesh method to the third order ADER scheme. We have the following results: 1) Third order convergence is successfully achieved. 2) Better results are obtained, i.e., oscillations are reduced and shock structures are better resolved, on simulations of Euler equations. 3) All simulations in this paper are stable for large CFL number. 4) The number of grid points is greatly reduced, avoiding of solving the problem on a very dense mesh, which saves the memory.

Acknowledgments

The research work of Yaguang Gu is partially supported by Postgraduate Studentship of University of Macau. The research work of Yaguang Gu and Guanghui Hu is partially supported by FDCT 050/2014/A1, MYRG2014-00109-FST, and National Natural Science Foundation of China (Grant No. 11401608).

https://doi.org/10.4208/cicp.OA-2016-0088 Published online by Cambridge University Press

References

[1] B. Fryxell, `http://cococubed.asu.edu/codes/riemann/exact_riemann.f`.

[2] R. Borges, M. Carmona, B. Costa, and W. S. Don, An improved weighted essentially non-oscillatory scheme for hyperbolic conservation laws, J. Comput. Phys., 227(6):3191–3211, 2008.

[3] W. M. Cao, W. Z. Huang and R. D. Russell, A study of monitor functions for two-dimensional adaptive mesh generation, SIAM J. Sci. Comput., 20(6):1978–1994, 1999.

[4] J. Bo. Cheng, E. F. Toro, S. Jiang, and W. J. Tang, A sub-cell WENO reconstruction method for spatial derivatives in the ADER scheme, J. Comput. Phys., 251:53–80, 2013.

[5] P. G. Ciarlet, The finite element method for elliptic problems, volume 40, SIAM, 2002.

[6] B. Cockburn, B. Dong, J. Guzmán, M. Restelli, and R. Sacco, A hybridizable discontinuous Galerkin method for steady-state convection-diffusion-reaction problems, SIAM J. Sci. Comput., 31(5):3827–3846, 2009.

[7] B. Cockburn and C.-W. Shu, TVB Runge-Kutta local projection discontinuous Galerkin finite element method for conservation laws. II. General framework, Math. Comp., 52(186):411–435, 1989.

[8] B. Cockburn and W. J. Zhang, A posteriori error analysis for hybridizable discontinuous Galerkin methods for second order elliptic problems, SIAM J. Numer. Anal., 51(1):676–693, 2013.

[9] A. Gelb and E. Tadmor, Adaptive edge detectors for piecewise smooth data based on the minmod limiter, J. Sci. Comput., 28(2-3):279–306, 2006.

[10] S. Gottlieb and C.-W. Shu, Total variation diminishing Runge-Kutta schemes, Math. Comp., 67(221):73–85, 1998.

[11] F. X. Hu, R. Wang, X. Y. Chen, and H. Feng, An adaptive mesh method for 1D hyperbolic conservation laws, Appl. Numer. Math., 91:11–25, 2015.

[12] G. H. Hu, An adaptive finite volume method for 2D steady Euler equations with WENO reconstruction, J. Comput. Phys., 252:591–605, 2013.

[13] G. H. Hu, R. Li, and T. Tang, A robust high-order residual distribution type scheme for steady Euler equations on unstructured grids, J. Comput. Phys., 229(5):1681–1697, 2010.

[14] G. H. Hu, R. Li, and T. Tang, A robust WENO type finite volume solver for steady Euler equations on unstructured grids, Commun. Comput. Phys., 9(3):627–648, 2011.

[15] W. Z. Huang and R. D. Russell, Moving mesh strategy based on a gradient flow equation for two-dimensional problems, SIAM J. Sci. Comput., 20(3):998–1015, 1998.

[16] X. Ji, H. Z. Tang, High-order accurate Runge-Kutta (local) discontinuous Galerkin methods for one-and two-dimensional fractional diffusion equations, Numer. Math. Theor. Meth. Appl., 5(3):333–358, 2012.

[17] G.-S. Jiang and C.-W. Shu, Efficient implementation of weighted ENO schemes, Technical report, DTIC Document, 1995.

[18] R. Kannan and Z. J. Wang, Improving the high order spectral volume formulation using a diffusion regulator, Commun. Comput. Phys., 12(01):247–260, 2012.

[19] R. Kannan and Z. J. Wang, A high order spectral volume solution to the Burgers' equation using the Hopf–Cole transformation, Internat. J. Numer. Methods Fluids, 69(4):781–801, 2012.

[20] L. Krivodonova, Limiters for high-order discontinuous Galerkin methods, J. Comput. Phys., 226(1):879–896, 2007.

[21] R. J. LeVeque, Finite volume methods for hyperbolic problems, volume 31, Cambridge Univ. Press, 2002.

https://doi.org/10.4208/cicp.OA-2016-0088 Published online by Cambridge University Press

[22] R. J. LeVeque, Numerical methods for conservation laws, volume 132, Birkhäuser Basel, 1992.
[23] R. Li, T. Tang, and P. W. Zhang, Moving mesh methods in multiple dimensions based on harmonic maps, J. Comput. Phys., 170(2):562–588, 2001.
[24] J. Liu, M. Goman, X. Li, and M. Liu, Positivity-preserving Runge-Kutta discontinuous Galerkin method on adaptive Cartesian grid for strong moving shock, Numer. Math. Theor. Meth. Appl., 9(1):87–110, 2016.
[25] R. C. Millington, V. A. Titarev, and E. F. Toro, H. Freistühler, G. Warnecke (Eds.) ADER: Arbitrary order non-oscillatory advection schemes hyperbolic problems: Theory, Numerics, Applications, volume 141:723–732, Birkhäuser Basel, 2001.
[26] N. C. Nguyen, J. Peraire, and B. Cockburn, A class of embedded discontinuous Galerkin methods for computational fluid dynamics, J. Comput. Phys., 302:674–692, 2015.
[27] J. X. Qiu and C.-W. Shu, Hermite WENO schemes and their application as limiters for Runge–Kutta discontinuous Galerkin method: one-dimensional case, J. Comput. Phys., 193(1):115–135, 2004.
[28] J. Remski, Mesh spacing estimates and efficiency considerations for moving mesh systems, Numer. Math. Theor. Meth. Appl., 9(3):432–450, 2016.
[29] C.-W. Shu, Essentially non-oscillatory and weighted essentially non-oscillatory schemes for hyperbolic conservation laws, Springer, 1998.
[30] H. Z. Tang and T. Tang, Adaptive mesh methods for one-and two-dimensional hyperbolic conservation laws, SIAM J. Numer. Anal., 41(2):487–515, 2003.
[31] V. A. Titarev and E. F. Toro, ADER schemes for three-dimensional non-linear hyperbolic systems, J. Comput. Phys., 204(2):715–736, 2005.
[32] V. A. Titarev and E. F. Toro, ADER: Arbitrary high order Godunov approach, J. Sci. Comput., 17(1-4):609–618, 2002.
[33] E. F. Toro, Riemann solvers and numerical methods for fluid dynamics: a practical introduction, Springer, 2009.
[34] E. F. Toro and V. A. Titarev, Derivative Riemann solvers for systems of conservation laws and ADER methods, J. Comput. Phys., 212(1):150–165, 2006.
[35] E. F. Toro and V. A. Titarev, Solution of the generalized Riemann problem for advection–reaction equations, Proc. Roy. Soc. London A, volume 458:271–281, 2002.
[36] C. Wang, X. X. Zhang, C.-W. Shu, and Jianguo Ning, Robust high order discontinuous Galerkin schemes for two-dimensional gaseous detonations, J. Comput. Phys., 231(2):653–665, 2012.
[37] Z. J. Wang, K. Fidkowski, R. Abgrall, F. Bassi, D. Caraeni, A. Cary, H. Deconinck, R. Hartmann, K. Hillewaert, H. T. Huynh, et al, High-order CFD methods: current status and perspective, Internat. J. Numer. Methods Fluids, 72(8):811–845, 2013.
[38] K. L. Wu and H. Z. Tang, Finite volume local evolution Galerkin method for two-dimensional relativistic hydrodynamics, J. Comput. Phys., 256:277–307, 2014.
[39] Q. Zhang and C.-W. Shu, Error estimates for the third order explicit Runge-Kutta discontinuous Galerkin method for a linear hyperbolic equation in one-dimension with discontinuous initial data, Numer. Math., 126(4):703–740, 2014.
[40] H. Q. Zhu and J. X. Qiu, Adaptive Runge–Kutta discontinuous Galerkin methods using different indicators: one-dimensional case, J. Comput. Phys., 228(18):6957–6976, 2009.

https://doi.org/10.4208/cicp.OA-2016-0088 Published online by Cambridge University Press